Supplementary materials.

Kiln scar mapping

We relied on a multisensor multitemporal dataset of high-resolution imagery to map the spatial distribution of charcoal kilns annually between 2013 and 2019. Kiln scars are patches of burnt soil created during the charcoal making process in the locations where kilns are built. They conform distinct features in high-resolution images, with low reflectance values in near infrared (NIR) (Smith et al., 2010; Chuvieco et al., 2019) and a significant spectral contrast with their immediate surrounding area. This spectral contrast remains visible for a period that can oscillate between few months and over a year depending on site conditions (Sedano et al., 2020b), enabling the detection of kiln scars as the basis of an indirect approach to monitoring forest degradation from charcoal production (Bolognesi et al., 2015; Dons et al., 2015; Sedano et al., 2016). Object detection methods for remote sensing optical images developed in the last decades can be labeled into four categories: template matching-based, knowledge-based, object-based image analysis and machine learning (Chen & Han, 2016). Region growing is a clustering approach in which pixels were grouped into spatially contiguous regions based on discontinuities in intensity level and other predefined criteria. While an object-based approach in essence, the proposed strategy relied on a priori knowledge of the charcoal production process to simplify the segmentation problem and improve the robustness of its results. In this sense, this approach combined elements from both knowledge-based and object-based image analysis methods (Chen & Han, 2016). This a priori knowledge was used at various stages of the process: Basic knowledge of the spectral signal and spatial context of kiln scars guided the seed identification. Field-based information of kiln size and shape served to establish criteria for region growth (Baltsavias, 2004). Knowledge of the charcoal production process in the study area aided to restrict the kiln scar detection to a specific land cover type. RG was applied on a single band basis, with NIR band as a default option. Initial exploratory work indicated that late dry season conditions (July - December) maximized the

spectral contrast between kiln scars and surrounding areas, and gradually declined with the offset of the rains, as tree leaves sprout, and vegetation covers the ground. Therefore, when available, late dry season images were used for the region growing process. Outside of the dry season, tree shadows present low NIR values, complicating the reliable detection of kiln scars. As an alternative, NDVI images were used when only rainy season (January - June) images were available. Input images were preprocessed to increase the contrast between kiln scars and neighboring pixels as an initial step for the definition of seeds:

$$E = \frac{(G - b_{NIR})}{b_{NIR}} \qquad [1]$$

where, *E* corresponded to the enhanced contrast image; b_{NIR} was the NIR band*;* and *G* the Gaussian filtered NIR image applying a 60 m radius kernel size established from field observations. Kiln scar locations corresponded to pixels with positive high contrast values, and seed pixels were subsequently selected as pixels with values below a threshold. This threshold was adaptively computed as the average of the first percentile of the pixel values in the mopane woodlands of all the images in a given epoch. Regions were grown from seeds based on spectral similarity with seed pixels and size and shape criteria defined from field observations in the study area (Sedano et al., 2020b). Additionally, a location criterion was implemented to avoid double counting of kiln scars in overlapping images and kiln scars detectable in images from several imagery epochs. Kiln scars were only registered when a kiln scar had not been previously mapped in that location in previous images, establishing a conservative vicinity buffer (kernel radius= 15 m) to account for potential image georegistration errors.

The approach was only implemented within the mopane woodlands in the study area because charcoal production takes place mostly in these woodland formations. These woodlands were identified in a 2011 mopane mask created using supervised classification of Landsat 8 images (Sedano et al., 2020a). Additionally, a bare soil mask was applied to minimize potential commission errors due to surfaces with

low NDVI values. This mask was created as the majority vote of an ensemble model from a set of masks created from the supervised classification of each imagery epoch using a combination of visual interpretation and field information as training data. The implementation of this region-based segmentation process retrieved kiln scar maps in the study area for each year between 2013 and 2019.

Small adjacent kilns (< 4 m long) are often built to use the logs that could not be fitted in the main kiln. Considering the spatial resolution of the imagery, it was assumed that adjacent kilns could not be confidently mapped throughout the study area and period. Fieldwork information, obtained from 323 sites visited in the field, indicated that 11.9 % of the kilns presented adjacent kilns. The final number of kilns per year included these adjacent kilns.

Kiln dimensions

A second region growing routine was implemented to extract kiln scar dimensions from very high-resolution (0.5 m) panchromatic WorldView1 imagery from the year 2014. This analysis was carried out in six sample locations with charcoal production activities, under the assumption that kiln construction patterns did not significantly change during the study period. The total area of these sites covered 154 km^2 and included 10,823 kiln scars. This region growing routine used the kiln scars detected in the previous kiln scar mapping as seed pixels and growth based on the spectral similarity between seed and neighboring pixels, size, and shape criteria. Subsequently, the two main axes of each region were calculated as an approximation to kiln scar dimensions (length and width). Finally, a histogram matching was implemented to calibrate image-based kiln scar dimensions to kiln dimensions measured in the field (n = 76).

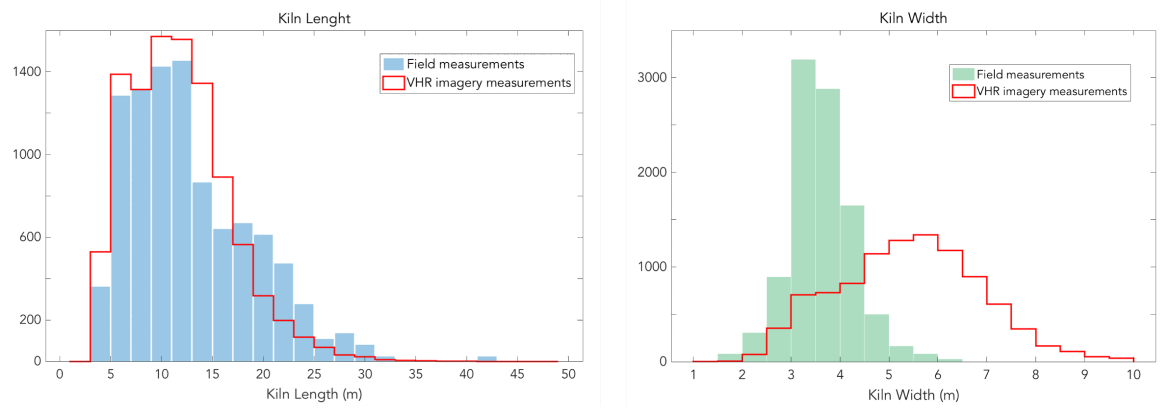

Figure 1. Comparison of histograms of kiln dimensions extracted from very high-resolution panchromatic WorldView 1 images and measured in the field.

Aboveground biomass removals

Annual AGB removals from charcoal production were calculated as the sum of the estimated wood biomass extracted to build all kilns mapped with the high-resolution imagery in the study area.

For each detected kiln scar, kiln wood biomass was estimated as a product of the kiln dimensions, its wood volume proportion, debris rate and wood density:

$$AGB_{EXT} = \sum_i^N (L_i \times W_i \times H_i) \times (1/(1-R)) \times T \times D \qquad [2]$$

where, AGB_{EXT} represents total annual aboveground biomass removals; *N* represents the number of kiln scars in the study area during a given period; L, W and H correspond to the length, width and height of kilns. Kiln length and width distributions were estimated from the analysis of very high-resolution imagery after a field data-based calibration (histogram matching). Kiln height distribution was built from field information. The dimensions were approximated to normal distributions N (11.45, 6.34), N (3.41, 0.69) and N (1.2, 0.2) for length, width and height respectively; *R* is the rate of debris (15.2 %), defined as the additional AGB left on site and not used in the kiln (e.g., small branches, twigs and leaves), obtained from previous studies in the region (Martins et al., 2016); *T* corresponds to the kiln wood volume proportion, fitted to a normal distribution N (78.52, 1.05) from information collected during a

field campaign in the study area (Sedano et al., 2020a); *D* is the mopane air-dry wood density, obtained from the literature as a fixed parameter at 1,080 kg/m^3 (Carsan et al., 2012).

Wood biomass for each kiln was estimated using Monte Carlo simulations (n = 100,000) to draw the values of each parameter from their respective statistical distributions.

Ecosystem Model

We used the Ecosystem Demography (ED) model (Moorcroft et al., 2001, Hurtt et al., 2002) to simulate potential biomass and extract relevant biomass trajectories for our study area for the region. ED is an individual-based, terrestrial biosphere model that uses a size and age-structured approximation of a gap model for modeling vegetation dynamics. By relying on these approximations, ED can simulate plant growth, phenology, mortality, belowground C and N dynamics and disturbance at the level of a single tree and scale up to an entire ecosystem to estimate changes in population structure and community composition, while simultaneously modeling natural disturbances, land use, and the ecosystem dynamics lands recovering from disturbances. ED offers an advantage over traditional Dynamic Global Vegetation Models (DGVMs) by combining the capacity of DGVMs to predict C dynamics at global scales with the fine-scale representation of ecological processes that can be performed by gap models. In ED, individual plants of different functional types compete mechanistically under local environmental conditions for light, water, and nutrients. These include C3 and C4 plants (as grasses), and early, mid and late successional species. ED divides the land surface under study into a sequence of 'patches' wherein each patch corresponds to a different age or stage of vegetation succession. Within each patch, cohorts of individual trees are organized. Each cohort has similar plant functional type and size and is represented mathematically as a single tree in the model. It is this mathematic simplification that gives ED its efficiency to operate at high resolution for large study areas. The model has been validated at multiple temporal and spatial scales and used for assessment of ecosystem dynamics in South and

Central America (Moorcroft et al., 2001), patterns of tree mortality and its drivers in northeastern North America (Dietze and Moorcroft, 2011), U.S. carbon sink (Pacala et al., 2001), and projections of its future, including the importance of future fire and fire suppression (Hurtt et al., 2002). The model has also been used to simulate post-disturbance re-growth under various scenarios of charcoal production in woodlands of central Mozambique (Silva et al., 2016). The model version used in this study is based on the original version designed to evaluate the effects of land-use change on U.S. carbon balance (Hurtt et al., 2002, Flanagan et al., 2016, 2019), with model modifications and parameterization to match regionally observed estimates of biomass and NPP. To run the ED model, we processed the following datasets (Flanagan et al., 2016, 2019):

Soils:

The World Inventory of Soil Emission (WISE) dataset is global in nature, with a spatial resolution of approximately 10km at the equator. Introduced in the 1990's (Batjes, 1996), it has grown in the number of soil properties available as well as filling in the missing information gaps globally (Batjes, 2005 and Batjes, 2009). It has been widely used to parameterize crop simulation models (Gijsman et al., 2007). We obtained soil depth information from WISE and use soil texture information from WISE to index a lookup table relating soil texture to saturated conductivity values (Cosby et al., 1984). ED uses a single soil-layer bucket model to simulate water percolation through the soil as mediated by the saturated conductivity of the soil.

Climate:

To determine the climatic inputs required by ED, we used the observation constrained CRUNCEP dataset (http://dods.extra.cea.fr/data/p529viov/cruncep/readme.htm). This dataset has been used in model inter-comparison projects and while relatively coarse resolution at half-degree, is global in scope (Huntzinger et al., 2013).

Further, we made the following adjustments to the model parameters to better match the observed growth rates and biomass trajectories in our study area:

1. *Parameterization and downregulation of carboxylation rate*

We adjusted the carboxylation rate (V_{cmax}) for each plant functional type (PFT). V_{cmax} controls the rate of carbon assimilation and respiration and is one of the most sensitive and poorly constrained parameters in earth system models (Rogers et al., 2014). Table 1 presents the original (Hurtt et al., 2002) and modified V_{cmax} values for each PFT. Our current V_{cmax} values are consistent with other earth system models (Albani et al., 2006)

PFT	Original	Current
C_4 grasses	37.5	12.5
C_3 grasses	37.5	12.5
Early successional	37.5	12.0
Mid successional	37.5	12.0
Late successional	37.5	7.0
Evergreen needle leaf	37.5	7.0
Cold deciduous	37.5	7.0

Table 1. Carboxylation rate (µmol $m^{-2}s^{-1}$) by PFT

We also incorporated mechanisms to downregulate V_{cmax} based on length of day and the leaf area index of the overhead canopy based on the community land model (CLM) (Lawrence et al., 2011). Downregulating based on day length introduces a seasonal variation in V_{cmax}, accounting for the lower

carbon assimilation in fall. Plants also tend to conserve rubisco, a key enzyme controlling V_{cmax}, by maximizing its production at the top of the canopy.

2. *Computation and parameterization of density-independent mortality*

Density-independent mortality takes into account the net carbon balance (net primary productivity minus maintenance demand) of a cohort to compute its probability of survival. Since, we are now downregulating V_{cmax} based on day length, effectively shutting down photosynthesis in fall in many regions across the globe, we extended the time-horizon to compute the carbon balance to an entire year.

We reparametrized density-independent mortality values in the southern hemisphere to better match regional estimates of biomass and NPP. A new term was added to the density-independent mortality calculation (0.015 yr^{-1}).

Charcoal production process – Images

The following images serve as a visual reference of charcoal production in the Mabalane district. A detailed description of description of the charcoal production process can be found in the supplementary Materials of Sedano et al. (2020a).

Figure 2: Mopane logs in under construction charcoal kiln (kiln longitudinal section)

Figure 3: Kiln under construction. Mopane logs in the process of being covered by branches and dirt.

Figure 4: Recent charcoal kiln scar.

Figure 5: Old charcoal kiln scar covered by vegetation.

Figure 6: Undisturbed mopane woodland.

Figure 7: Disturbed mopane woodlands after charcoal production.

Figure 8: Detail of mopane tree (*Colophospermum mopane*).

References

Baltsavias E P 2004 Object extraction and revision by image analysis using existing geodata and knowledge: Current status and steps towards operational systems *ISPRS J. Photogramm. Remote Sens.* **58** 129–51dons

Bolognesi M, Vrieling A, Rembold F and Gadain H 2015 Rapid mapping and impact estimation of illegal charcoal production in southern Somalia based on WorldView-1 imagery *Energy Sustain. Dev.* **25** 40–9

Carsan S, Orwa C, Harwood C, Kindt R, Stroebel A, Neufeldt H, and Jamnadass R. 2012. African Wood Density Database. World Agroforestry Centre, Nairobi.

Cheng G and Han J 2016 A survey on object detection in optical remote sensing images *ISPRS J. Photogramm. Remote Sens.* **117** 11–28

Chuvieco E, Mouillot F, van der Werf G R, San Miguel J, Tanase M, Koutsias N, García M, Yebra M, Padilla M, Gitas I, Heil A, Hawbaker T J and Giglio L 2019 Historical background and current developments for mapping burned area from satellite Earth observation *Remote Sens. Environ.* **225** 45–64

Dietze M C and Moorcroft P R 2011 Tree mortality in the eastern and central United States: patterns and drivers. Global Change Biology, 17(11), pp.3312-3326.

Dons K, Smith-Hall C, Meilby H and Fensholt R 2015 Operationalizing measurement of forest degradation: Identification and quantification of charcoal production in tropical dry forests using very high resolution satellite imagery *Int. J. Appl. Earth Obs. Geoinf.* **39** 18–27

Hurtt G C, Pacala S W, Moorcroft P R, Caspersen J, Shevliakova E, Houghton R A and Moore B I I I 2002 Projecting the future of the US carbon sink. Proceedings of the National Academy of Sciences, 99(3), pp.1389-1394.

Martins, M., Atanassov, B., Mirira R 2016 *Produção sustentável de carvão vegetal. Teoria e prática na definição, implementação e avaliação de formas de terra melhorados IBEK, não distrito de Mabalane - Província de Gaza*

Moorcroft P R, Hurtt G C, and Pacala S W 2001 A method for scaling vegetation dynamics: the ecosystem demography model (ED). Ecological monographs, 71(4), pp.557-586.

Pacala S W, Hurtt G C, Baker D, Peylin P, Houghton R A, Birdsey R A, Heath L, Sundquist E T, Stallard R F, Ciais P, and Moorcroft P 2001 Consistent land-and atmosphere-based US carbon sink estimates. Science, 292(5525), pp.2316-2320.

Sedano F, Silva J A, Machoco R, Meque C H, Sitoe A, Ribeiro N, Anderson K, Ombe Z A, Baule S H and Tucker C J 2016 The impact of charcoal production on forest degradation: A case study in Tete, Mozambique *Environ. Res. Lett.* **11**

Sedano F, Lisboa S N, Duncanson L, Ribeiro N, Sitoe A, Sahajpal R, Hurtt G and Tucker C J 2020a Monitoring forest degradation from charcoal production with historical Landsat imagery. A case study in southern Mozambique *Environ. Res. Lett.* **15** 015001

Sedano F, Lisboa S, Duncanson L, Ribeiro N, Sitoe A, Sahajpal R, Hurtt G and Tucker C 2020b Monitoring intra and inter annual dynamics of forest degradation from charcoal production in Southern Africa with Sentinel – 2 imagery *Int. J. Appl. Earth Obs. Geoinf.* **92** 102184

Silva J A, Sedano F, Flanagan S, Ombe Z A, Machoco R, Meque C H, Sitoe A, Ribeiro N, Anderson K, Baule S and Hurtt G 2019 Charcoal-related forest degradation dynamics in dry African woodlands: Evidence from Mozambique *Appl. Geogr.* **107** 72–81

Smith A M S, Eitel J U H and Hudak A T 2010 Spectral analysis of charcoal on soils: implications for wildland fire severity mapping methods *Int. J. Wildl. Fire Wildl. Fire* **19** 976–983 Online: www.publish.csiro.au/journals/ijwf